PAPER • OPEN ACCESS

Gapless quantum spin liquid in the S = 1/2 anisotropic kagome antiferromagnet $ZnCu_3(OH)_6SO_4$

To cite this article: Yuesheng Li *et al* 2014 *New J. Phys.* **16** 093011

View the article online for updates and enhancements.

Related content

- Structure and magnetism of S = 1/2 kagome antiferromagnets NiCu3(OH)6Cl2 and CoCu3(OH)6Cl2
  Yue-sheng Li and Qing-ming Zhang

- Cluster spin glass behavior in geometrically frustrated Zn3V3O8
  T Chakrabarty, A V Mahajan and S Kundu

- Quantum frustration in organic Mott insulators
  B J Powell and Ross H McKenzie

Recent citations

- Magnetic and transport properties of Mn2FeAl
  I. Gavrikov *et al*

- Recent progress on magnetic-field studies on quantum-spin-liquid candidates
  Zhen Ma *et al*

- Rare-Earth Chalcogenides: A Large Family of Triangular Lattice Spin Liquid Candidates
  Weiwei Liu *et al*

Gapless quantum spin liquid in the S = 1/2 anisotropic kagome antiferromagnet ZnCu₃(OH)₆SO₄

Yuesheng Li[1], Bingying Pan[2], Shiyan Li[2], Wei Tong[3], Langsheng Ling[3], Zhaorong Yang[4], Junfeng Wang[5], Zhongjun Chen[6], Zhonghua Wu[6] and Qingming Zhang[1]

[1] Department of Physics, Renmin University of China, Beijing 100872, People's Republic of China
[2] State Key Laboratory of Surface Physics, Department of Physics, and Laboratory of Advanced Materials, Fudan University, Shanghai 200433, People's Republic of China
[3] High Magnetic Field Laboratory, Hefei Institutes of Physical Science, Chinese Academy of Sciences, Hefei 230031, People's Republic of China
[4] Key Laboratory of Materials Physics, Institute of Solid State Physics, Chinese Academy of Sciences, Hefei 230031, People's Republic of China
[5] Wuhan National high magnetic field center, Wuhan 430074, People's Republic of China
[6] Institute of High Energy Physics, Chinese Academy of Science, Beijing 100049, People's Republic of China
E-mail: qmzhang@ruc.edu.cn

Abstract

We have successfully synthesized the new $S = 1/2$ anisotropic kagome antiferromagnet $ZnCu_3(OH)_6SO_4$ and determined its structure by synchrotron x-ray diffraction. No magnetic ordering is observed down to $50\,mK$, despite a moderately high Weiss temperature of $\Theta_w \sim -79\,K$, indicating that the compound is a new quantum spin liquid (QSL) candidate. A linear temperature dependence of the magnetic heat capacity is found at $6 \sim 15\,K$ and below $0.6\,K$. Temperature-independent intrinsic susceptibilities are observed exactly in both temperature ranges. This consistently suggests a gapless QSL below $0.6\,K$, which may evolve from an unconventional quantum spin state at higher temperatures $(6 \sim 15\,K)$.

Introduction

The ground state and low-energy excitations of a frustrated spin system have attracted a great deal of interest in condensed matter physics [1–4]. The strongest spin frustration was considered to occur in a $S = 1/2$ kagome Heisenberg antiferromagnet (KHA), on which extensive theoretical studies were performed and many novel quantum spin liquid (QSL) ground states were proposed [5–10]. Fermi-liquid-like low-energy excitations, such as the linear temperature dependence of heat capacity and/or temperature-independent susceptibility, are experimentally observed in most reported QSL candidate compounds. These excitations are attributed to spinons, fractional particle excitations in gapless spin liquids [11–14].

One of the current key issues in the field is to search for new QSL candidates. Two promising $S = 1/2$ KHA candidates have been reported so far. One is a vanadium-based organic compound with $S = 1$ interlayer ions [15, 16]. The other one is the famous herbertsmithite $ZnCu_3(OH)_6Cl_2$ [17–22]. In the latter compound, a small mixing of magnetic Cu^{2+} and non-magnetic Zn^{2+} between kagome and interlayer sites, and the Dzyaloshinskii–Moriya (DM) interaction, which is a measure of spin–orbit coupling, were reported [23].

$ZnCu_3(OH)_6Cl_2$ was synthesized by replacing 25% of Cu^{2+} ions in clinoatacamite $Cu_4(OH)_6Cl_2$ (Neel temperature $T_c \sim 7.5$ K) with Zn^{2+}. The site preferences drive Zn^{2+} ions to enter interlayer sites and Cu^{2+} ions to occupy kagome sites [24–26]. In this paper we tried a similar substitution in the recently synthesized brochantite $Cu_4(OH)_6SO_4$, which has four symmetrically inequivalent Cu sites forming corrugated distorted triangular 2D planes and shows a long-range Neel ordering at 7.5 K [27]. When one of the four Cu sites (Cu4) in $Cu_4(OH)_6SO_4$ was successfully replaced by Zn^{2+}, we obtained a new $S = 1/2$ anisotropic kagome antiferromagnet $ZnCu_3(OH)_6SO_4$ with well magnetically separated corrugated 2D planes. Unlike herbertsmithite, both Cu^{2+} and Zn^{2+} ions in the new compound are located in the anisotropic kagome planes. For a fixed number of spins in 2D planes, from less-frustrated edge-sharing triangular to vertex-sharing kagome lattices, the number of constraints is minimized, and the ground-state degeneracy is maximized [28]. Naturally an obvious suppression of long-range Neel ordering and a much stronger spin frustration should be expected.

Magnetization and heat capacity measurements reveal some exciting features in the compound. No magnetic ordering was observed, even down to 50 mK. The Weiss temperature of $\Theta_w \sim -79$ K gives a degree of spin frustration, $f = |\Theta_w|/T_c$, [4, 28] higher than ~1580. The two linear temperature-dependent behaviors in magnetic heat capacity exactly correspond to the temperature-independent intrinsic susceptibilities at $6 \sim 15$ K and below 0.6 K. Both the linear heat capacity coefficients (γ) and temperature-independent intrinsic susceptibilities (χ) are proportional to the density of low-energy states, which may be attributed to spinons, electrons or other quasi-particles with a 'pseudo-Fermi surface' [4]. Considering that the compound is a good insulator with a gap of 4.2 eV, the quantum spin state below 0.6 K seems compatible with the resonating valence bond (RVB) QSL with a 'pseudo-Fermi surface' [2, 3]. It may evolve

from the unusual quantum state at higher temperatures ($6 \sim 15$ K) through a rapid crossover, possibly driven by spin–orbit coupling, anisotropic nearest neighboring interactions or other higher order interactions.

Methods

$ZnCu_3(OH)_6SO_4$, $Zn_{0.6}Cu_{3.4}(OH)_6SO_4$ and $Cu_4(OH)_6SO_4$ powder samples were prepared by hydrothermal synthesis from an aqueous suspension obtained from $CuSO_4 \cdot 5H_2O$, NaOH and $ZnSO_4 \cdot 7H_2O$ in H_2O (see the supplementary information, available from stacks.iop.org/NJP/16/093011/mmedia). Inductively coupled plasma (ICP) measurements were performed with a Horiba Jobin Yvon Ultima 2 ICP system. The measured ratios of Zn:Cu are 0.91(5): 3.09 in $ZnCu_3(OH)_6SO_4$ and 0.58(3): 3.42 in $Zn_{0.6}Cu_{3.4}(OH)_6SO_4$. The ratios of Zn:Cu are determined to be 1.05(5): 2.95 in $ZnCu_3(OH)_6SO_4$ and 0.68(5): 3.32 in $Zn_{0.6}Cu_{3.4}(OH)_6SO_4$ with a scanning electron microscope–x-ray energy dispersive spectrometer (SEM–EDX, JEOL JSM-6700F). Synchrotron x-ray diffractions (XRD) and x-ray absorption fine structure (XAFS) spectra were performed in the diffraction station (4B9A) of Beijing Synchrotron Radiation Facility (BSRF). The powder sample of ~200 mg for synchrotron XRD was pressed into the $1\,cm \times 1\,cm \times 1.5\,mm$ square groove of a glass slide. A tape evenly coated with the powder sample, ~10 mg, was used for synchrotron XAFS. The General Structure Analysis System (GSAS) program was used for Rietveld refinements [29]. The ultraviolet/visible (UV/VIS) absorption spectrum for $ZnCu_3(OH)_6SO_4$ was measured using a PerkinElmer Lambda 950 with a deuterium lamp. The powder sample, ~10 mg, was tightly and evenly clamped by two quartz slides for the UV/VIS absorption experiment. High-pulsed-field (up to 42 T) magnetization measurements were performed at Wuhan Pulsed High Magnetic Field Center (WHMFC). Magnetization and heat capacity measurements above 2 K were made with Quantum Design MPMS and PPMS, respectively. Magnetization measurements between 2 K and 0.5 K were made with a Quantum Design SQUID with a ^{3}He system. Heat capacities between 3.6 K and 50 mK were measured using a Quantum Design PPMS with a dilution refrigerator system, on a 1.7 mg dye-pressed pellet of $ZnCu_3(OH)_6SO_4$. The international system of units (SI) is used.

Results

Synchrotron x-ray powder diffraction and Rietveld refinement for $ZnCu_3(OH)_6SO_4$ are shown in figure 1(a). No additional peak is observed, indicating negligible impurity phases in the sample. $ZnCu_3(OH)_6SO_4$ has a monoclinic structure with the space group P 21/a, a = 13.0606 (12) Å, b = 9.8697(10) Å, c = 6.0882(6) Å, and $\beta = 103.6071(24)^o$, similar to the parent $Cu_4(OH)_6SO_4$ [27]. One of the four inequivalent Cu sites (Cu4) in $Cu_4(OH)_6SO_4$ is dominantly replaced (~78%) by Zn (see the supplementary information), as synchrotron resonant XRD, XAFS and combined Rietveld refinements revealed [30]. The ∠CuOCu bond angles characterizing nearest neighboring exchange couplings [27, 31, 32] are shown in figure 1(b). In figures 1(b) and (c), two non-equivalent chains along the *c*-axis can be clearly seen. Edge-sharing copper octahedrons (CuO_6) line up along the first chain (A), and the other chain (B) is an alternate alignment of zinc planes (ZnO_4) and copper octahedrons (CuO_6). The chains are AB-stacked along the *b*-axis to form corrugated kagome planes with 6% distortions of Cu–Cu bonds (figure 1(d)). The corrugated Cu^{2+} S = 1/2 kagome planes are well magnetically separated
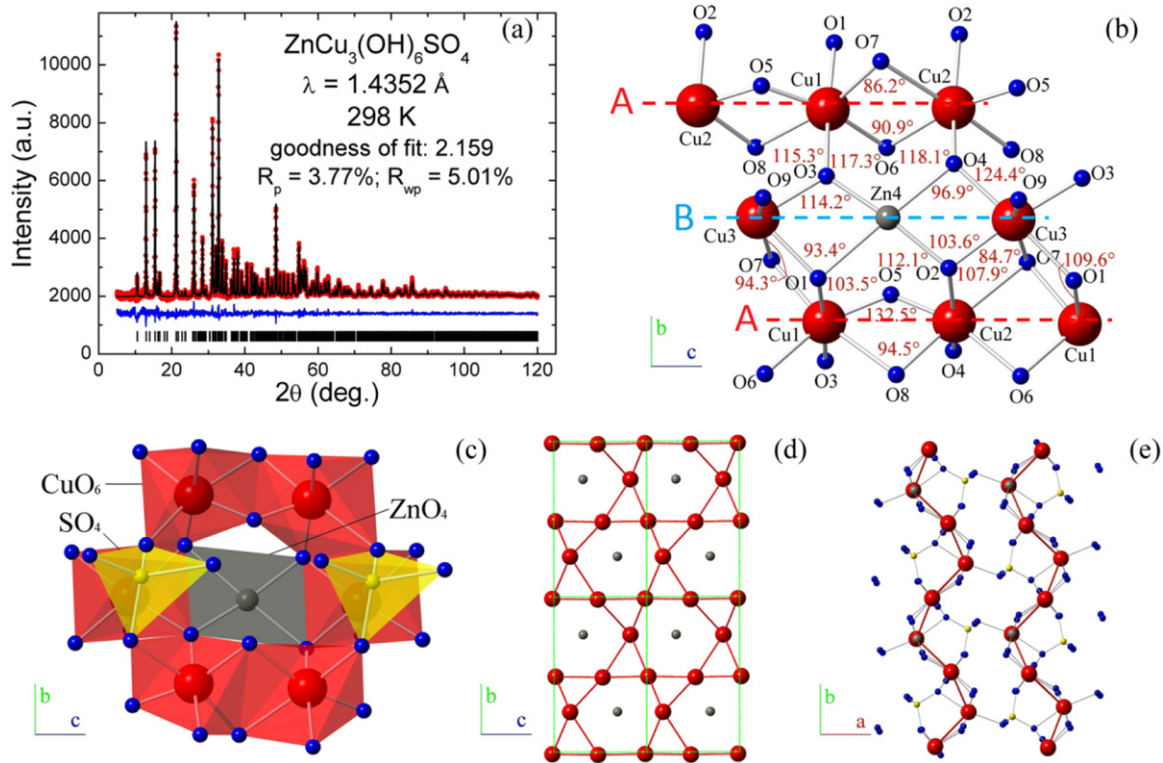
Figure 1. (a) Synchrotron x-ray powder diffraction and Rietveld refinement for $ZnCu_3(OH)_6SO_4$ with a incident light of $h\upsilon = 8639\,eV$, $\lambda = 1.4352\,Å$, at room temperature. (b) Top view of $ZnCu_3(OH)_6SO_4$ along the *a* axis. All inequivalent sites, $\angle CuO(Cu, Zn)$ bond angles and chains A/B are labeled. Here sulphur (S) and hydrogen (H) atoms are omitted for simplification, while only hydrogen atoms are omitted in (c) and (e). (c) The polyhedral structure of $ZnCu_3(OH)_6SO_4$ in the bc plane. (d) The Cu^{2+} S = 1/2 kagome network projected on the bc plane. Green lines show the unit cells. Only Cu/Zn sites are shown for simplification. (e) Top view of $ZnCu_3(OH)_6SO_4$ along the *c* axis. The Cu^{2+} S = 1/2 kagome planes are corrugated along the *b* axis and are well magnetically separated along the *a* axis.

by non-magnetic SO_4 tetrahedrons (figure 1(e)). As a building block of kagome lattices, each spin triangle consists of three non-equivalent nearest Cu^{2+} ions, suggesting anisotropic spin interactions. Refinements give a ~8% site disorder between Cu^{2+} and Zn^{2+}, which is further confirmed by magnetization and heat capacity measurements (see below).

We have synthesized three samples with Zn = 0, 0.6 and 1.0. All of the samples are good insulators with a room-temperature resistance higher than $20\,M\Omega$. The UV/VIS absorption spectrum of $ZnCu_3(OH)_6SO_4$ gives a large band gap Eg of ~4.2 eV. the dc susceptibilities are shown in figure 2(a). The high temperature (150 ~ 300 K) Currie–Weiss fitted parameters are summarized in table 1. The Lande g factors, obtained from the fitted Curie constants, are in accord with the typical value of Cu^{2+} [23]. The magnetizations under zero field cooling (ZFC) and field cooling (FC, 100 Oe) are shown in figure 2(b). A clear splitting between FC and ZFC in $Cu_4(OH)_6SO_4$ occurs around $T_c \sim 7.5\,K$, indicating a long-range Neel transition [27] and a moderate degree of spin frustration $f = |\Theta_w|/T_c \sim 13$ for parent triangular lattices [4]. The transition temperature is suppressed to 3.5 K in $Zn_{0.6}Cu_{3.4}(OH)_6SO_4$ and f is pushed up to ~26.
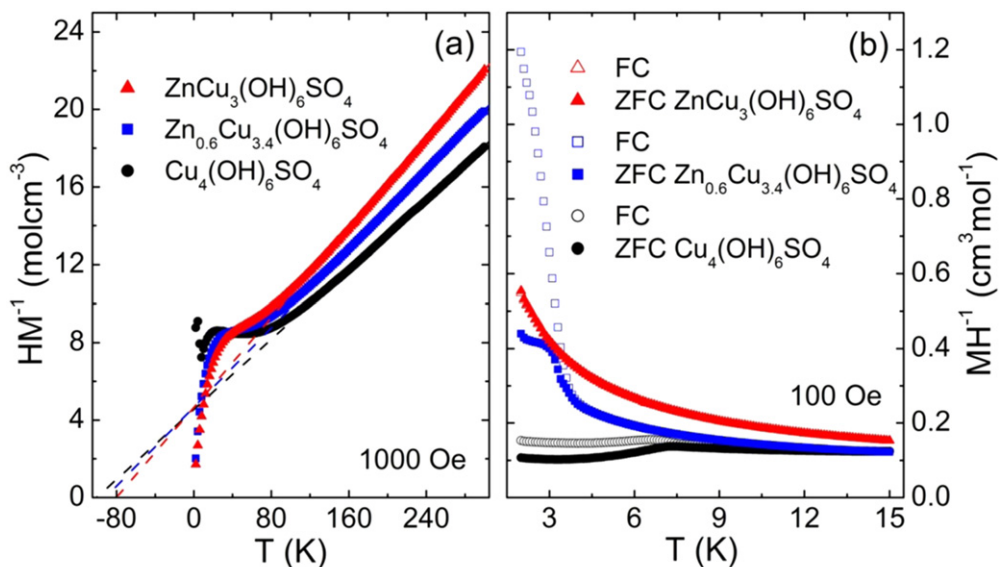
Figure 2. Magnetization measurements for the three samples. (a) HM^{-1} versus T measured under 1000 Oe at $2 \sim 300$ K. The colored dashed lines are linear fits (Curie–Weiss) from 150 K to 300 K. (b) MH^{-1} versus T measured under zero field cooling and field cooling (100 Oe) with a measurement field of 100 Oe at $2 \sim 15$ K. For $ZnCu_3(OH)_6SO_4$, the FC curve (red open triangles) is completely overlapped by the ZFC one (red solid triangles).

Table 1. High temperature $(150 \sim 300$ K) Curie–Weiss fitted parameters, transition temperatures and frustration factors for the three samples.

Zn_xCu_{4-x} $(OH)_6SO_4$	Weiss temperature (K)	transition temperature (K)	frustration factor ($|\Theta_w|/T_c$)	Curie constant $(K cm^3/mol)$	μ_{eff} (μ_B/Cu)	g
x = 0	−100	7.5	13	22.2	1.88	2.17
x = 0.6	−90	3.5	26	19.5	1.91	2.21
x = 1	−79	<0.05	>1580	17.1	1.90	2.20

The splitting in the partially Zn-substituted compound could originate from an AF or a spin-glass transition [33]. The splitting completely disappears in $ZnCu_3(OH)_6SO_4$. Further magnetization and heat capacity measurements (see below) indicate that no magnetic transition is found, even down to 50 mK ($f > 1580$). This demonstrates that strong spin frustration in brochantite systems is successfully realized through non-magnetic ion substitution.

Magnetization measurements were made under high pulsed magnetic fields (up to 42 T) at 4.2 K and static fields (up to 6 T) at 0.5 K (figures 3(a) and (b)). Magnetization saturation occurs ~ 20 T at 4.2 K and ~ 4.5 T at 0.5 K, respectively [16, 34]. Above the saturation fields, the magnetizations exhibit a linear field-dependence with the slopes of $\chi_{up}(4.2$ K$) \sim 0.08$ cm^3 mol^{-1} and $\chi_{up}(0.5$ K$) \sim 0.26$ cm^3 mol^{-1}. By subtracting the linear contributions ($\chi_{up}H$), $\sim 8\%$ quasi-free spins can be consistently estimated at both temperatures, in agreement with the above refinement results. The quasi-free spins are often attributed to magnetic defects due to a small Zn–Cu mixing [34, 35]. Disordered magnetic defects Cu^{2+} (Cu4) and the integrated staggered
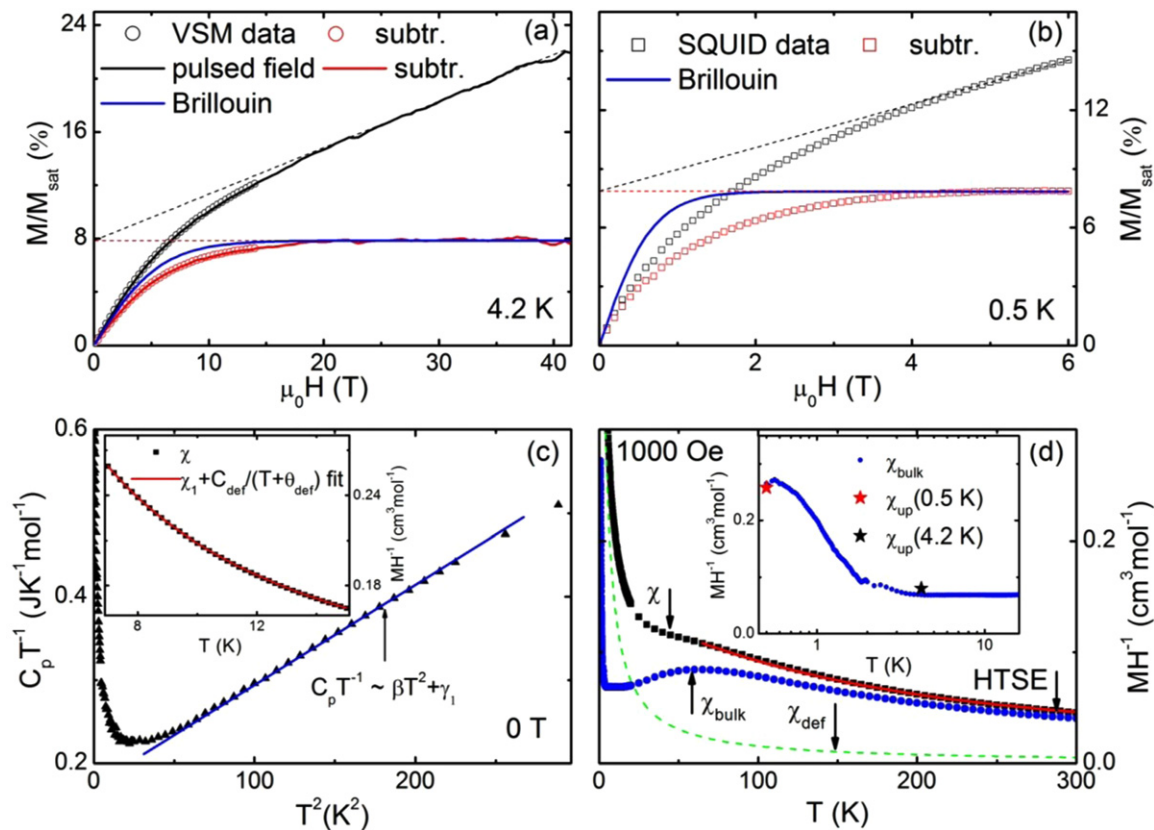
Figure 3. Magnetization of $ZnCu_3(OH)_6SO_4$ measured at 4.2 K under a high pulsed field (a) and at 0.5 K under static fields by SQUID (b). (a) The high pulsed field data (up to 42 T, the black curve) are normalized by PPMS–VSM measurements (up to 14 T, black circles). In (a) and (b), the black dashed lines are linear fits under high fields. The data labeled 'subtr.' are obtained by subtracting the linear contributions from the total measured magnetizations. The blue curves labeled 'Brillouin' are Brillouin functions with ~8% free spins (S = 1/2). The red dashed lines are a guide to the eye. (c) The zero-field heat capacity of $ZnCu_3(OH)_6SO_4$. The blue line is the linear fit from 7 to 15 K. Inset: Susceptibility fitting from 7 to 15 K with a constant plus a Curie–Weiss term. (d) Susceptibility under 1000 Oe. the red curve is a high-temperature series expansion (HTSE) simulation. Inset: A comparison between intrinsic bulk susceptibilities and the values (χ_{up}) extracted from the M–H curve at 0.5 K and 4.2 K.

magnetization around kagome nonmagnetic defects Zn^{2+} can contribute to these quasi-free spins [36]. The magnetizations from defect spins can be well described by Brillouin functions at 4.2 K and 0.5 K, except for a small overshooting at low fields, which suggests that defect spins are somehow coupled rather than completely free [16, 34].

Schottky contributions to the zero-field heat capacity from quasi-free defect spins become negligible at 7 ~ 15 K (see also below, $\Delta_{0T}/k_B \ll 7$ K). Thus the total heat capacity can be safely decomposed into lattice and intrinsic (magnetic or electronic) contributions. Figure 3(c) shows the zero-field heat capacity from 7 to 15 K, which can be well fitted with a T term plus a T^3 term: $C_p = \beta T^3 + \gamma_1 T$, where $\beta \sim 1.18(1)$ mJ K^{-4} mol^{-1} and $\gamma_1 \sim _177(1)$ mJ K^{-2} mol^{-1}. The T^3 term comes from lattice vibrations (see below), while the linear term is generally attributed to gapless QSL with a 'pseudo-Fermi surface' or electronic specific heat. Physically, the linear

heat capacity corresponds to the temperature-independent susceptibility (χ_1) in the same temperature range [4]. Therefore, the measured susceptibility can be decomposed into two parts: the intrinsic susceptibility χ_1 and the contributions from the magnetic defects $\chi_{def} = C_{def}/(T-\Theta_{def})$ [34, 37, 38] (inset of figure 3(c)). It gives ~9% weakly coupled rather than completely free S = 1/2 defect spins with a Weiss temperature $\Theta_{def} \sim -1.16(1)$ K [34, 37, 38]. By subtracting the magnetic defect contributions from the total susceptibilities, we further obtain bulk susceptibilities dominantly contributed by frustrated spins (figure 3(d)). With cooling down, a broad hump of bulk susceptibilities develops around $|\Theta_w|$, suggesting a short-range magnetic correlation in kagome planes [37, 38]. Bulk susceptibilities are nearly temperature-independent with $\chi_1 \sim 0.068$ cm³ mol⁻¹ from 6 to 15 K, and they quickly rise with further cooling down. A blurred but still visible maximum $\chi_2 \sim 0.27$ cm³ mol⁻¹ is reached below 0.6 K (inset of figure 3(d)). The slopes $\chi_{up}(4.2$ K) and $\chi_{up}(0.5$ K) extracted from figures 3(a) and (b) are in good agreement with the bulk susceptibilities. This indicates that our data analysis is self-consistent and bulk susceptibilities are contributed by intrinsic magnetic excitations. By applying an S = 1/2 KHA high-temperature series expansion (HTSE) simulation to the high temperature part (>150 K) of the measured susceptibilities with g ∼ 2.20 (figure 3(d)), an average effective antiferromagnetic coupling can be estimated to be $J_{eff} \sim 65$ K [14, 38, 39].

Heat capacity measurements down to 50 mK were performed to probe low-energy excitations. No sharp peak structure is observed (figure 4(a)), suggesting the absence of long-range spin ordering. The broad peak at several Kelvins shifts to higher temperatures when applying magnetic fields. It is a typical Schottky anomaly arising from magnetic defects, as often found in some SL candidates [13, 14, 16, 40]. The difference between 0 T and 12 T data can be well modeled by Zeeman splitting for S = 1/2 spins (figure 4(b)). The Schottky term can be written as $f_d[C_{sch}(\Delta_{H1})-C_{sch}(\Delta_{H2})]/T$, where $C_{sch}(\Delta_H)$ is the heat capacity from an S = 1/2 spin with an energy splitting Δ_H, and f_d is the fraction of doublets per formula. The fitted f_d (~0.184 (2)) gives 6.1(1) % defect spins. The value is a little smaller than ~8% given by the above refinements and magnetization measurements. A similar discrepancy is also found in ZnCu₃(OH)₆Cl₂ [34, 37, 40, 41] and remains an open question. For free spins, Δ_H is expected to exactly follow Zeeman splitting with g ∼ 2.20 (inset of figure 4(b)). The slight difference may be due to a small coupling between quasi-free spins, as suggested in magnetization measurements. The zero-field splitting, $\Delta_{0T}/k_B \sim 1.4$ K, confirms that defect spins are weakly coupled rather than completely free. It explains why the Schottky anomaly is still observed under zero field around ~0.6 K (figure 4(a)). It should be noted that a tiny Schottky contribution from hydrogen nuclear spins appears below 80 mK (figures 4(a) and (d)). The term is centered below 50 mK and its high-temperature wing can be well simulated by AT^{-2} (figure 4(d)), where $A \sim 6.6(2) \times 10^{-2}$ mJ K mol⁻¹, in good accord with κ-(BEDT-TTF)₂Cu₂(CN)₃ and EtMe₃Sb[Pd (dmit)₂]₂ [11, 12].

We have measured the heat capacity up to 60 K for ZnCu₃(OH)₆SO₄ and Zn₀.₆Cu₃.₄(OH)₆SO₄ (figure 4(c)). Lattice contributions become dominant and the magnetic heat capacity is negligible at T > 45 K. Both heat capacities merge together due to the structural similarity. We apply the original Debye function with a Debye temperature ~225 K, to fit the lattice heat capacity at T > 45 K (figure 4(c)). Below 20 K, the discrepancy between standard Debye fitting and the T³-law is less than 1%, suggesting that we can safely use βT^3 to fit the lattice heat capacity at low temperatures (<15 K). This allows us to extract the intrinsic magnetic heat capacity after subtracting lattice contributions and the part contributed by magnetic defects, as shown in figure 4(d). Interestingly, two linear behaviors with $\gamma_1 \sim 177(1)$ mJ K⁻² mol⁻¹ and
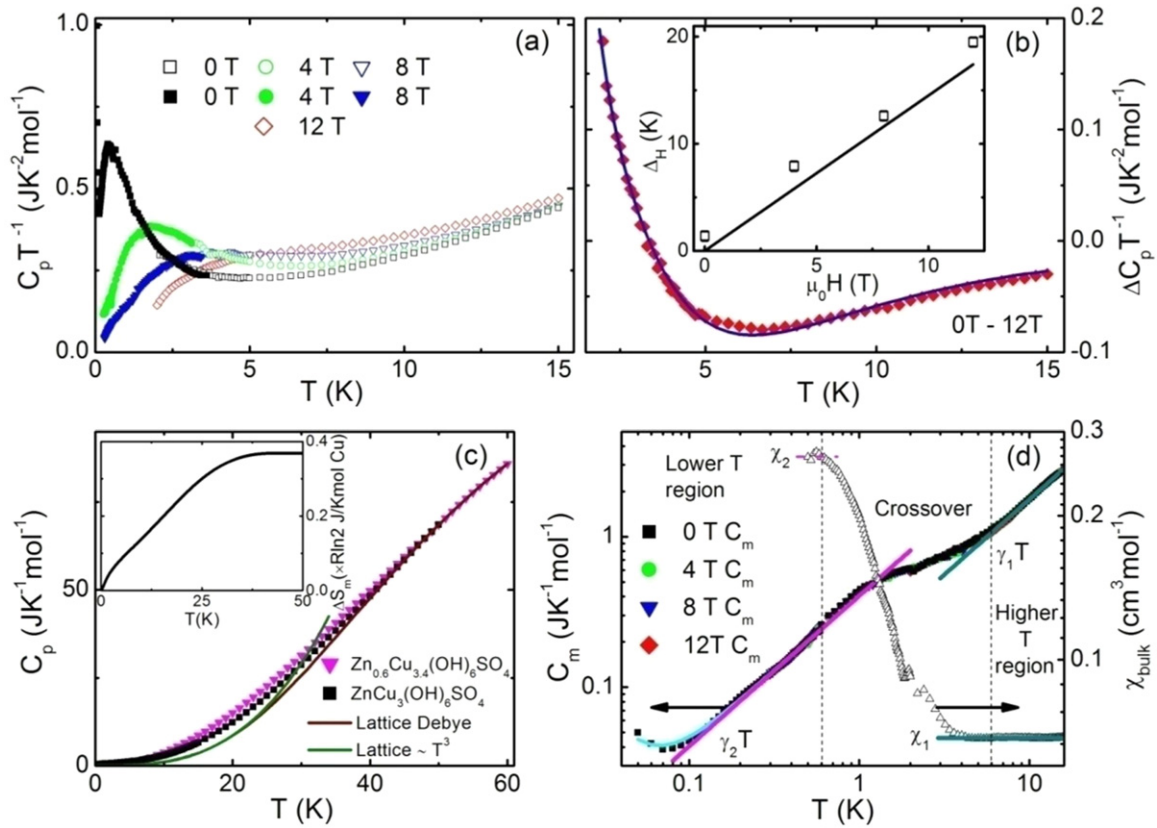
Figure 4. (a) Heat capacities measured under magnetic fields. Open and closed symbols correspond to PPMS measurements with liquid ^{4}He refrigeration and a dilution refrigerator system, respectively. (b) The difference between heat capacities under 0 T and 12 T, $[C_p(0\,T)-C_p(12\,T)]/T$. The blue curve is the Schottky simulation. Inset: open squares are the energy-level splitting Δ_H obtained from the heat capacity and the solid line is the Zeeman splitting for $S = 1/2$ free spins with $g \sim 2.20$. (c) Heat capacities of Zn = 1 and 0.6 samples under 0 T. Inset: the intrinsic magnetic entropy increase $\Delta S_m(T)$ starting from 50 mK for a Zn = 1 sample. (d) The intrinsic magnetic heat capacities and bulk susceptibilities. Cyan curve: the simulation including a Schottky term from hydrogen atoms $(\gamma_2 T + A/T^2)$ from 50 mK to 0.6 K.

$\gamma_2 \sim 405(4)$ mJ K^{-2} mol^{-1} appear at $6 \sim 15$ K and below 0.6 K, respectively. We further calculate the intrinsic magnetic entropy increase ΔS_m from 50 mK to 50 K (inset of figure 4(c)), which gives a $\sim 63(3)\%$ residual entropy of the total Cu^{2+} contributions. The residual entropy reflects the unfreezable part of the total degree of freedom of spins, and clearly suggests a ground state with macroscopic degeneracy in the new compound.

Discussion

The linear heat capacity coefficient at $0.05 \sim 0.6$ K (γ_2) is comparable to those of other inorganic QSL candidates such as Ba$_3$NiSb$_2$O$_9$ (6H-B) and ZnCu$_3$(OH)$_6$Cl$_2$ (table 2). At such low temperatures, the linear term is reasonably attributed to a gapless QSL with a 'pseudo-Fermi surface', considering that the compound is a good insulator [4]. The picture seems compatible

Table 2. Linear heat capacity coefficients, temperature ranges for linear heat capacity, and Wilson ratios in $ZnCu_3(OH)_6SO_4$ and other reported QSL candidates.

Compound	Linear heat capacity coefficient	Temperature range for linear heat capacity	Wilson ratio R_w
κ-(BEDT-TTF)$_2$Cu$_2$(CN)$_3$ [11]	20 ± 5 mJ K^{-2} mol^{-1}	$0.075 \sim 3$ K ($3 \times 10^{-4} \sim 1.2 \times 10^{-2}$ J)	1.8 [4] or 1.13 [12]
EtMe$_3$Sb[Pd(dmit)$_2$]$_2$ [12]	19.9 mJ K^{-2} mol^{-1}	$0.9 \sim 2.0$ K ($3.8 \times 10^{-3} \sim 8.5 \times 10^{-3}$ J)	1.09
Ba$_3$CuSb$_2$O$_9$ [14]	43.4 mJ K^{-2} mol Cu	$0.35 \sim 1.4$ K ($6.4 \times 10^{-3} \sim 2.6 \times 10^{-2}$ $|\Theta_w|$)	?
Ba$_3$NiSb$_2$O$_9$(6H-B) [13]	168 mJ K^{-2} mol Ni	$0.35 \sim 7$ K ($4.6 \times 10^{-3} \sim 9.3 \times 10^{-2}$ $|\Theta_w|$)	5.6
ZnCu$_3$(OH)$_6$Cl$_2$ [41]	240 ± 20 mJ K^{-2} mol Cu	$106 \sim 400$ mK	?
ZnCu$_3$(OH)$_6$SO$_4$(higher temperature region) This work	59 mJ K^{-2} mol Cu (177(1) mJ K^{-2} mol^{-1})	$6 \sim 15$ K ($7.6 \times 10^{-2} \sim 1.9 \times 10^{-1}$ $|\Theta_w|$)	1.9
ZnCu$_3$(OH)$_6$SO$_4$(lower temperature region) This work	135(1) mJ K^{-2} mol Cu (405(4) mJ K^{-2} mol^{-1})	0.05–0.6 K ($6.3 \times 10^{-4} \sim 7.6 \times 10^{-3}$ $|\Theta_w|$)	3.2

with the RVB QSL with a 'pseudo-Fermi surface' [2, 3] rather than a valence-bond crystal (VBC) [9], the gapped Z_2 [5] and gapless U(1) Dirac [6, 7] (where $C \sim T^2$ and $\chi \sim T$) SL ground states of HKA.

The linear behavior at higher temperatures ($6 \sim 15$ K) is a little more complicated to understand, as the temperature range seems relatively high for QSL compared with other QSL candidates (table 2). One possibility is the effect of thermal fluctuations. We have also tried $\beta T^3 + aT^2$ to fit the heat capacity under 0 T at the temperature region (not shown here). But it fails to follow the experimental data. The temperature-independent susceptibilities (χ_1) observed in the same temperature range (figure 4(d)) are also hard to understand in terms of classical thermal spin fluctuations. Another possibility is electronic origin, which should correspond to a weak Pauli paramagnetism in nature. The linear coefficient (γ_1) seems too large for a conventional metal, in which the typical Sommerfeld coefficient ranges from 0.1 to 10 mJ K^{-2} mol^{-1}. One may argue that it may be caused by a large effective electron mass. The smaller Wilson ratio at $6 \sim 15$ K, $R_W = 4\pi^2 k_B^2 \chi/(3 g^2 \mu_0 \mu_B^2 \gamma) \sim 1.9$ also looks consistent with this possibility. However, the linear term rising from electrons is nearly zero considering that the compound is a good insulator with a large gap of ~ 4.2 eV and that the density of free electrons is extremely low.

On the other hand, the temperature range of $6 \sim 15$ K is still very low (<0.19 $|\Theta_w|$) compared with $|\Theta_w|$ or J_{eff}. As a result, quantum spin fluctuations may be strong enough to overcome classical thermal spin fluctuations, and a QSL state still possibly survives [4]. Both γ and χ below 0.6 K are several times larger than those at $6 \sim 15$ K. This indicates that the density

of low-energy quantum states are much enhanced as cooling down. We can further compare Wilson ratios in both temperature ranges, which are considered to be a quantitative description on the importance of spin–orbit coupling [4]. They are $R_{W1} \sim 1.9$ and $R_{W2} \sim 3.2$ in the higher- and lower-T regions, respectively. The remarkable increase of R_W at low temperatures suggests an enhanced importance of spin–orbit coupling. This becomes possible because the high-order interactions, such as spin–orbit coupling and anisotropic nearest neighboring exchange interaction, may stand out due to the gradual suppression of thermal spin fluctuations at low temperatures. Hence it may result in an enhanced density of low-energy quantum states below $0.6\,K$ in $ZnCu_3(OH)_6SO_4$. The unconventional behaviors at $6 \sim 15\,K$ may be also caused by other unknown magnetic or quasi-particle excitations with a 'pseudo-Fermi surface'. To unravel the underlying physics, further theoretical and experimental studies are required in the future.

Conclusion

In conclusion, we have synthesized a new QSL candidate $ZnCu_3(OH)_6SO_4$, which has corrugated but well-magnetically-separated $S = 1/2$ kagome planes. No magnetic ordering is observed, even down to $50\,mK$ ($f > 1580$). The linear temperature dependence of the intrinsic magnetic heat capacity is observed in the ranges of $6 \sim 15\,K$ and below $0.6\,K$, while the corresponding bulk susceptibilities are temperature-independent. The observations suggest that a gapless QSL appears at low temperatures ($T < 0.6\,K$), which may evolve from an unconventional quantum spin state at $6 \sim 15\,K$ with much enhanced density of low-energy states. The understanding of the present observations brings new challenges for the existing theoretical scenarios and is expected to yield new insights into QSL.

Acknowledgments

Reference

[1] Anderson P W 1973 Resonating valence bonds—new kind of insulator *Mater. Res. Bull.* **8** 153–60
[2] Anderson P W 1987 The resonating valence bond state in La$_2$CuO$_4$ and superconductivity *Science* **235** 1196–8
[3] Anderson P W, Baskaran G, Zou Z and Hsu T 1987 Resonating-valence-bond theory of phase transitions and superconductivity in La$_2$CuO$_4$-based compounds *Phys. Rev. Lett.* **58** 2790–3
[4] Balents L 2010 Spin liquids in frustrated magnets *Nature* **464** 199–208
[5] Yan S, Huse D A and White S R 2011 Spin-liquid ground state of the $S = 1/2$ kagome Heisenberg antiferromagnet *Science* **332** 1173–6
[6] Ran Y, Hermele M, Lee P A and Wen X G 2007 Projected-wave-function study of the spin-1/2 Heisenberg model on the kagome lattice *Phys. Rev. Lett.* **98** 117205
[7] Hermele M, Ran Y, Lee P A and Wen X G 2008 Properties of an algebraic spin liquid on the kagome lattice *Phys. Rev. B* **77** 224413

[8] Iqbal Y, Becca F, Sorella S and Poilblanc D 2013 Gapless spin-liquid phase in the kagome spin-1/2 Heisenberg antiferromagnet *Phys. Rev.* B **87** 060405(R)

[9] Evenbly G and Vidal G 2010 Frustrated antiferromagnets with entanglement renormalization: ground state of the spin-1/2 Heisenberg model on a kagome lattice *Phys. Rev. Lett.* **104** 187203

[10] Jiang H C, Weng Z Y and Sheng D N 2008 Density matrix renormalization group numerical study of the kagome antiferromagnet *Phys. Rev. Lett.* **101** 117203

[11] Yamashita S, Nakazawa Y, Oguni M, Oshima Y, Nojiri H, Shimizu Y, Miyagawa K and Kanoda K 2008 Thermodynamic properties of a spin-1/2 spin-liquid state in a κ-type organic salt *Nat. Phys.* **4** 459–62

[12] Yamashita S, Yamamoto T, Nakazawa Y, Tamura M and Kato R 2011 Gapless spin liquid of an organic triangular compound evidenced by thermodynamic measurements *Nat. Commun.* **2** 275

[13] Cheng J G, Li G, Balicas L, Zhou J S, Goodenough J B, Xu C and Zhou H D 2011 High-pressure sequence of $Ba_3NiSb_2O_9$ structural phases: new S = 1 quantum spin liquids based on Ni^{2+} *Phys. Rev. Lett.* **107** 197204

[14] Zhou H D, Choi E S, Li G, Balicas L, Wiebe C R, Qiu Y, Copley J R D and Gardner J S 2011 Spin liquid state in the S = 1/2 triangular lattice $Ba_3CuSb_2O_9$ *Phys. Rev. Lett.* **106** 147204

[15] Aidoudi F H, Aldous D W, Goff R J, Slawin A M Z, Attfield J P, Morris R E and Lightfoot P 2011 An ionothermally prepared S = 1/2 vanadium oxyfluoride kagome lattice *Nat. Chem.* **3** 801

[16] Clark L *et al* 2013 Gapless spin liquid ground state in the S = 1/2 vanadium oxyfluoride kagome antiferromagnet $[NH_4]_2[C_7H_{14}N][V_7O_6F_{18}]$ *Phys. Rev. Lett.* **110** 207208

[17] Braithwaite R S W, Mereiter K, Paar W H and Clark A M 2004 Herbertsmithite, $Cu_3Zn(OH)_6Cl_2$, a new species, and the definition of paratacamite *Mineral. Mag.* **68** 527–39

[18] Shores M P, Nytko E A, Bartlett B M and Nocera D G 2005 A structurally perfect S = 1/2 kagome antiferromagnet *J. Am. Chem. Soc.* **127** 13462–3

[19] Lee P A 2008 An end to the drought of quantum spin liquids *Science* **321** 1306–7

[20] de Vries M A, Stewart J R, Deen P P, Piatek J O, Nilsen G J, Rønnow H M and Harrison A 2009 Scale-free antiferromagnetic fluctuations in the S = 1/2 kagome antiferromagnet Herbertsmithite *Phys. Rev. Lett.* **103** 237201

[21] Han T H, Helton J S, Chu S, Nocera D G, Rodriguez-Rivera J A, Broholm C and Lee Y S 2012 Fractionalized excitations in the spin-liquid state of a kagome-lattice antiferromagnet *Nature* **492** 406–10

[22] Olariu A, Mendels P, Bert F, Duc F, Trombe J C, de Vries M A and Harrison A 2008 ^{17}O NMR study of the intrinsic magnetic susceptibility and spin dynamics of the quantum kagome antiferromagnet $ZnCu_3(OH)_6Cl_2$ *Phys. Rev. Lett.* **100** 087202

[23] Zorko A, Nellutla S, van Tol J, Brunel L C, Bert F, Duc F, Trombe J C, de Vries M A, Harrison A and Mendels P 2008 Dzyaloshinsky-Moriya anisotropy in the spin-1/2 kagome compound $ZnCu_3(OH)_6Cl_2$ *Phys. Rev. Lett.* **101** 026405

[24] Mendels P, Bert F, de Vries M A, Olariu A, Harrison A, Duc F, Trombe J C, Lord J S, Amato A and Baines C 2007 Quantum magnetism in the paratacamite family: towards an ideal kagome lattice *Phys. Rev. Lett.* **98** 077204

[25] Lee S H, Kikuchi H, Qiu Y, Lake B, Huang Q, Habicht K and Kiefer K 2007 Quantum-spin-liquid states in the two-demensional kagome antiferromagnets $Zn_xCu_{4-x}(OD)_6Cl_2$ *Nat. Mater.* **6** 853–7

[26] Wills A S, Raymond S and Henry J Y 2004 Magnetic ordering in a distorted S = 1/2 pyrochlore antiferromagnet *J. Magn. Magn. Mater.* **272-276** 850–1

[27] Vilminot S, Richard-Plouet M, André G, Swierczynski D, Bourée-Vigneron F and Kurmoo M 2006 Nuclear and magnetic structures and magnetic properties of synthetic brochantite, $Cu_4(OH)_6SO_4$ *Dalton Trans.* **11** 1455–62

[28] Moessner R and Ramirez A P 2006 Geometrical frustration *Phys. Today* **59** 24–9

[29] Larson A C and Von Dreele R B 2004 General structure analysis system (GSAS) *Report No.* LAUR 86-748 (Los Alamos, NM: Los Alamos National Laboratory)

[30] Li Y S, Fu J L, Wu Z H and Zhang Q M 2013 Transition-metal distribution in kagome antiferromagnet $CoCu_3(OH)_6Cl_2$ revealed by resonant X-ray diffraction *Chem. Phys. Lett.* **570** 37–41

[31] Mizuno Y, Tohyama T, Maekawa S, Osafune T, Motoyama N, Eisaki H and Uchida S 1998 Electronic states and magnetic properties of edge-sharing Cu–O chains *Phys. Rev.* B **57** 5326–35

[32] Tornow S, Entin-Wohlman O and Aharony A 1999 Anisotropic superexchange for nearest and next-nearest coppers in chain, ladder, and lamellar cuprates *Phys. Rev.* B **60** 10206–15

[33] Li Y S and Zhang Q M 2013 Structure and magnetism of S = 1/2 kagome antiferromagnets NiCu$_3$(OH)$_6$Cl$_2$ and CoCu$_3$(OH)$_6$Cl$_2$ *J. Phys.: Condens. Matter* **25** 026003

[34] Bert F, Nakamae S, Ladieu F, L'Hôte D, Bonville P, Duc F, Trombe J C and Mendels P 2007 Low temperature magnetization of the S = 1/2 kagome antiferromagnet ZnCu$_3$(OH)$_6$Cl$_2$ *Phys. Rev.* B **76** 132411

[35] Fåk B *et al* 2012 Kapellasite: A kagome quantum spin liquid with competing interactions *Phys. Rev. Lett.* **109** 037208

[36] Rousochatzakis I, Manmana S R, Läuchli A M, Normand B and Mila F 2009 Dzyaloshinskii–Moriya anisotropy and nonmagnetic impurities in the S = 1/2 kagome system ZnCu$_3$(OH)$_6$Cl$_2$ *Phys. Rev.* B **79** 214415

[37] Hiroi Z, Yoshida H, Okamoto Y and Takigawa M 2009 Spin-1/2 kagome compounds: volborthite *vs* herbertsmithite *J. Phys.: Conf. Ser.* **145** 012002

[38] Okamoto Y, Yoshida H and Hiroi Z 2009 Vesignieite BaCu$_3$V$_2$O$_8$(OH)$_2$ as a candidate spin-1/2 kagome antiferromagnet *J. Phys. Soc. Jpn.* **78** 033701

[39] Elstner N and Young A P 1994 Spin-1/2 Heisenberg antiferromagnet on the kagome lattice: High-temperature expansion and exact-diagonalization studies *Phys. Rev.* B **50** 6871–6

[40] de Vries M A, Kamenev K V, Kockelmann W A, Sanchez-Benitez J and Harrison A 2008 Magnetic ground state of an experimental S = 1/2 kagome antiferromagnet *Phys. Rev. Lett.* **100** 157205

[41] Helton J S *et al* 2007 Spin dynamics of the spin-1/2 kagome lattice antiferromagnet ZnCu$_3$(OH)$_6$Cl$_2$ *Phys. Rev. Lett.* **98** 107204